PERGAMON

International Journal of Solids and Structures 40 (2003) 5229–5249

INTERNATIONAL JOURNAL OF SOLIDS and STRUCTURES

www.elsevier.com/locate/ijsolstr

A meshfree method for transverse vibrations of anisotropic plates

G. Davì *, A. Milazzo

Dipartimento di Ingegneria Aeronautica e dei Trasporti, University of Palermo, Viale delle Scienze, 90128 Palermo, Italy

Received 9 May 2003; received in revised form 9 May 2003

Abstract

A meshfree approach, called displacement boundary method, for anisotropic Kirchhoff plate dynamic analysis is presented. This method is deduced from a variational principle, which uses a modified hybrid functional involving the generalized displacements and generalized tractions on the boundary and the lateral deflection in the domain as independent variables. The discretization process is based on the employment of the fundamental solutions of the static problem operator for the expression of the variables involved in the functional. The stiffness and mass matrices obtained for the dynamic model are frequency-independent, symmetric and positive definite and their computation involves boundary integrals of regular kernels only. Due to its features, the final resolving system can be solved with the classical approaches by using standard numerical procedures. To assess the formulation, the free vibrations of some anisotropic plates were calculated and the results compared with those obtained using other solution techniques. The present results are in good agreement with those found in the literature showing the accuracy and effectiveness of the proposed approach.

Keywords: Meshless methods; Meshfree methods; Anisotropic plate dynamics; Numerical methods

1. Introduction

Composite materials are widely employed in the new lightweight structure technology for the construction of many structural members such as multilayered plates and shells. Usually, these structures have complex geometries and layups in order to meet specific design requirements and this leads to an anisotropic global behavior, which is generally characterized by bending–stretching coupling. Then, the structural dynamic analysis plays a crucial role in the design and tailoring of this kind of structures in order to obtain the desired response. In this context, for the widespread case of thin composite plate and shell-like structures, the Kirchhoff theory provides a well established framework to accurately determine through-thickness averaged quantities such as deflections, stress resultants, buckling loads and natural frequencies.

* Corresponding author. Tel.: +39-91-6459905; fax: +39-91-485439.
E-mail address: davi@unipa.it (G. Davì).

0020-7683/$ - see front matter © 2003 Elsevier Ltd. All rights reserved.
doi:10.1016/S0020-7683(03)00293-2

Nomenclature

$\mathscr{D}$, $\boldsymbol{\Xi}$, $\boldsymbol{\Theta}$ generalized strain and equilibrium differential operators
$\mathbf{E}$ generalized elasticity matrix
f_i^* companion solution
h plate thickness
$\mathbf{K}$ stiffness matrix
M_{ij} $(i,j=1,2)$ bending and twisting moments
M_{n} boundary normal bending moment
M_{nt} boundary twisting moment
$\mathbf{M}$ mass matrix
NC number of corner points
NC_2 number of corner points on the free boundary
N number of discretization nodes
N_{B}, N_{D} number of discretization nodes on the boundary and in the domain
$\mathbf{N}$, $\boldsymbol{\Psi}$ shape function matrices
$\mathbf{N}_{wi}$, $\mathbf{N}_{\phi i}$ $(i=1,2)$ deflection and rotation shape function matrices
$\mathbf{p}$ nodal generalized tractions
$\mathbf{P}^*$ trial functions generalized tractions matrix
q plate transverse load
q_i^* trial function load
$\mathbf{Q}^*$ trial functions load matrix
T_{eq} Kirchhoff's shear force
$\mathbf{s}$ trial functions coefficient vector
$\tilde{\mathbf{t}}$ generalized tractions on the plate boundary
$\tilde{\mathbf{u}}$ generalized displacements on the plate boundary
w plate deflection
w_i^* trial function
$\mathbf{W}^*$, $\mathbf{U}^*$ trial functions displacement matrices
x_i $(i=1,2,3)$ Cartesian coordinates
$\boldsymbol{\delta}$ nodal generalized displacements
$\boldsymbol{\delta}_1$, $\boldsymbol{\delta}_2$ constrained and free nodal generalized displacements
$\boldsymbol{\delta}_\Gamma$, $\boldsymbol{\delta}_\Omega$ boundary and domain nodal generalized displacements
Γ_1, Γ_2, Γ constrained, free and entire plate boundary
κ_{ij} $(i,j=1,2)$ plate curvatures
μ_k fundamental solution eigenvalues
ρ plate density
$\boldsymbol{\sigma}$ generalized stress vector
Ω plate domain

Many authors have investigated this class of problems employing different techniques to describe and determine the static and dynamic response of anisotropic plates under various conditions. For the dynamic plate problem, both numerical and analytical solutions are available in the literature. Analytical solutions are generally given in terms of series expansion and they are restricted to simple geometries and boundary conditions (Hearmon, 1959; Lekhnitskii, 1968; Rossi et al., 1998; Kabir et al., 2001). Complex anisotropic plate configurations have been treated by numerical methods and many solutions have been obtained by

using the finite element method, which however has been developed for the analysis with higher order theories particularly suitable for thick plates (Noor and Burton, 1989; Reddy and Robbins, 1994; Liew et al., 1995). These finite element approaches require a fine mesh to obtain accurate results and this leads to high computational costs especially in the solution of problems involving structural constraints such as weight optimization and design limitations. From the beginnings, the boundary element method has been employed for plate analysis and solutions are available for both isotropic and anisotropic plates (Wu and Altiero, 1981; Irschik, 1984; Shi and Bezine, 1988; Providakis and Beskos, 1999). More recently, novel computational algorithms, referred as "meshless" or "meshfree" methods, have been proposed. These methods do not require a mesh for the interpolation of the solution variables but generally they involve shadow elements for integration purposes only (Monaghan, 1982; Liszka, 1984; Kansa, 1990; Nayroles et al., 1992; Belytschko et al., 1994, 1996; Liu et al., 1995; Zhu et al., 1999; Chati et al., 1999; Atluri and Zhu, 2000; Zhang et al., 2002; Liew et al., 2002a,b,c,d,e). The above-mentioned feature alleviates the difficulty of meshing and remeshing the entire structure whose discretization characteristics are changed by only adding or deleting nodes. Some of the proposed meshfree methods have been applied to plate analysis and in particular the element-free Galerkin method (Krysl and Belytschko, 1995), radial basis functions and Hermite collocation (Leitao, 2001) and the meshfree local boundary integral equation method (Shuyao, 2002). In the border between the boundary element method and the meshfree methods, the authors have recently proposed a novel approach called displacement boundary method (DBM), which has been successfully applied to 2D free and forced vibration analysis (Davì and Milazzo, 1994, 1997a) and to several problems involving isotropic plate dynamics (Davì and Milazzo, 1997b; Davì et al., 1997). In the framework of boundary element methods, the DBM represents a variational approach proposed in order to preserve the fundamental properties of symmetry and definiteness of the structural operators, which are lost in the classical boundary element method with the consequent theoretical and numerical drawbacks. On the other hand, the inherent structure of the approach makes it a "meshfree" method because only a set of scattered points is needed for the variable interpolation, whereas an underlying boundary mesh is used for the integration of the influence coefficients only. In this paper a model for the dynamic analysis of thin anisotropic plates is obtained when the DBM is used, which has been successfully applied to the static analysis of orthotropic plates (Davì and Milazzo, 1999). The problem governing equations are obtained from a hybrid functional originally proposed by De Figueredo and Brebbia (1989) for static elasticity problems and extended to plate flexural problems by the authors (Davì and Milazzo, 1997b; Davì et al., 1997). This hybrid functional is expressed in terms of the plate basic variables. On the boundary these are the generalized displacements, i.e. deflection and normal slope, and the generalized tractions, i.e. normal bending and Kirchhoff's shear force per unit length, whereas in the domain the functional involves the deflection only. These variables are assumed as independent of one another. The discretization process is based on the modelization of the internal displacement field by a superposition of static fundamental solutions of the anisotropic plate bending problem and the ensuing expressions for the boundary variables. The resolving equations are deduced from the stationarity conditions of the functional and they constitute a system of constant coefficients ordinary differential equations expressed in terms of nodal displacements. The stiffness and mass matrices involved in the model are frequency-independent and they preserve the symmetry and definiteness properties of the continuum. They are computed by running boundary integrations of regular kernels. Due to its features, the resolving system is solvable by efficient standard numerical procedures.

2. Definitions and basic equations

Consider a thin, anisotropic elastic plate and let its stretching and bending be uncoupled, e.g. symmetric composite laminate (Vasiliev, 1993). Under these assumptions, the deflection mode behavior of the plate

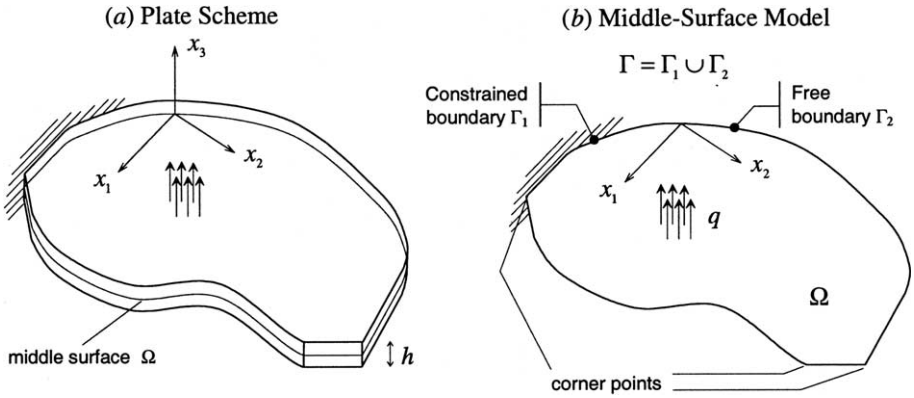

Fig. 1. Plate configuration and notation.

can be described on the basis of Kirchhoff's small deflection theory. To this purpose, a rectangular Cartesian coordinate system (x_1-, x_2- and x_3-axis) is considered to represent the plate geometry (see Fig. 1). The x_1–x_2 plane is placed at the mid-surface of the plate of thickness h, while the axis x_3 is normal to it. Again, let Ω denote the region of the x_1–x_2 plane occupied by the plate middle surface, which is bounded by the contour Γ having a constrained part Γ_1 and a free part Γ_2. The contour outer normal is denoted by n, and let $w = w(x_1, x_2, t)$ be the plate deflection. From Kirchhoff's theory of thin plates, the generalized strain–displacement relation, that is the curvature–deflection relationship, is defined as

$$\boldsymbol{\kappa} = \begin{bmatrix} \kappa_{11} \\ \kappa_{22} \\ \kappa_{12} \end{bmatrix} = -\mathscr{D} w \tag{1}$$

where the κ_{ij} ($i, j = 1, 2$) are the bending and twisting curvatures and the operator $\mathscr{D}$ is given by

$$\mathscr{D} = \begin{bmatrix} \frac{\partial^2}{\partial x_1^2} \\ \frac{\partial^2}{\partial x_2^2} \\ 2\frac{\partial^2}{\partial x_1 \partial x_2} \end{bmatrix} = \begin{bmatrix} \frac{\partial}{\partial x_1} & 0 \\ 0 & \frac{\partial}{\partial x_2} \\ \frac{\partial}{\partial x_2} & \frac{\partial}{\partial x_1} \end{bmatrix} \begin{bmatrix} \frac{\partial}{\partial x_1} \\ \frac{\partial}{\partial x_2} \end{bmatrix} = \boldsymbol{\Xi\Theta} \tag{2}$$

The corresponding generalized stresses are the usual bending moments around the x_1- and x_2-axes and the twisting moment per unit length, which can be expressed as

$$\boldsymbol{\sigma} = \begin{bmatrix} M_{11} \\ M_{22} \\ M_{12} \end{bmatrix} = \mathbf{E}\boldsymbol{\kappa} \tag{3}$$

The generalized elasticity matrix $\mathbf{E}$ is given by

$$\mathbf{E} = \begin{bmatrix} D_{11} & D_{12} & D_{16} \\ D_{12} & D_{22} & D_{26} \\ D_{16} & D_{26} & D_{66} \end{bmatrix} \tag{4}$$

where the constants D_{ij} are the bending and twisting rigidities that can be computed according to Lekhnitskii (1968) for both single-layer and multi-layer plates. By using the notation introduced above, the equilibrium equation governing the plate motion is written as

$$\mathscr{D}^{\mathrm{T}}\mathbf{E}\mathscr{D}w = q - \rho h\ddot{w} \tag{5}$$

where the right-hand side is the sum of the applied pressures q and the transverse inertia forces $\rho h\ddot{w}$. The Eq. (5) is the anisotropic biharmonic equation, which characterizes the plate dynamic response in terms of the transverse deflection w when the appropriate boundary and initial conditions are assigned. On the constrained boundary Γ_1, the kinematical boundary conditions are prescribed in terms of the boundary generalized displacements $\mathbf{u}$ whose components are the deflection and the normal slope. One has

$$\mathbf{u} = \begin{bmatrix} w \\ -\frac{\partial w}{\partial n} \end{bmatrix} = \bar{\mathbf{u}} \quad \text{on } \Gamma_1 \tag{6}$$

where the overbar denotes prescribed quantities. On the free boundary Γ_2, the mechanical boundary conditions are prescribed in terms of the generalized traction vector $\mathbf{t}$ whose components are the Kirchhoff's shear force T_{eq} and the normal bending M_{n}. They can be written as

$$\mathbf{t} = \begin{bmatrix} T_{\mathrm{eq}} \\ M_{\mathrm{n}} \end{bmatrix} = \bar{\mathbf{t}} \quad \text{on } \Gamma_2 \tag{7}$$

Moreover, for a plate with NC corners, the mechanical boundary conditions have to be supplemented by the corner conditions

$$\|M_{\mathrm{nt}}\|_i = \|\overline{M}_{\mathrm{nt}}\|_i \quad i = 1, \ldots, \mathrm{NC}_2 \tag{8}$$

where NC_2 is the number of free corner points and $\|M_{\mathrm{nt}}\|_i$ denotes the corner force due to the jump of the twisting moment at the ith corner on Γ_2. Finally, the deflection w is also subjected to the initial conditions given by

$$w(x_1, x_2, 0) = \bar{w}(x_1, x_2) \tag{9}$$

$$\dot{w}(x_1, x_2, 0) = \bar{\dot{w}}(x_1, x_2) \tag{10}$$

3. Modified variational principle

The dynamic model presented is based on a modified variational principle (De Figueredo and Brebbia, 1989) whose form for plate bending analysis has been previously introduced by the authors for the isotropic case (Davì and Milazzo, 1997b; Davì et al., 1997). In the following, the fundamentals of this variational principle are recollected to apply it to anisotropic plates. Let w be the lateral deflection of the plate in the domain Ω and let $\tilde{\mathbf{u}}$ and $\tilde{\mathbf{t}}$ be the boundary generalized displacements and tractions, respectively. The functions w, $\tilde{\mathbf{u}}$ and $\tilde{\mathbf{t}}$ are assumed to be independent one from each other. The corresponding hybrid variational functional for plates is defined as follows

$$\begin{aligned} \Pi = \int_\Omega \left[\frac{1}{2}\boldsymbol{\kappa}^{\mathrm{T}}\mathbf{E}\boldsymbol{\kappa} - w(q - \rho h\ddot{w}) \right] \mathrm{d}\Omega - \int_\Gamma (\mathbf{u} - \tilde{\mathbf{u}})^{\mathrm{T}}\tilde{\mathbf{t}}\,\mathrm{d}\Gamma - \int_{\Gamma_2} \tilde{\mathbf{u}}^{\mathrm{T}}\bar{\mathbf{t}}\,\mathrm{d}\Gamma + \sum_{i=1}^{\mathrm{NC}} \langle (w - \tilde{w}) \|\tilde{M}_{\mathrm{nt}}\| \rangle_i \\ + \sum_{i=1}^{\mathrm{NC}_2} \langle \tilde{w} \|\overline{M}_{\mathrm{nt}}\| \rangle_i \end{aligned} \tag{11}$$

By carrying out the variations, after integrating by parts and taking the essential boundary conditions on Γ_1 into account, it results

$$\partial\Pi = \int_{\Omega} [\mathscr{D}^{\mathrm{T}}\mathbf{E}\mathscr{D}w - q + \rho h\ddot{w}]^{\mathrm{T}}\partial w \,\mathrm{d}\Omega - \int_{\Gamma} (\mathbf{u} - \tilde{\mathbf{u}})^{\mathrm{T}}\partial\tilde{\mathbf{t}} \,\mathrm{d}\Gamma + \int_{\Gamma} (\mathbf{t} - \tilde{\mathbf{t}})^{\mathrm{T}}\partial\mathbf{u} \,\mathrm{d}\Gamma - \int_{\Gamma_2} (\bar{\mathbf{t}} - \tilde{\mathbf{t}})^{\mathrm{T}}\partial\tilde{\mathbf{u}} \,\mathrm{d}\Gamma$$
$$- \sum_{i=1}^{\mathrm{NC}} \langle (\|M_{\mathrm{nt}}\| - \|\tilde{M}_{\mathrm{nt}}\|)\partial w \rangle_i - \sum_{i=1}^{\mathrm{NC}_2} \langle (\|\tilde{M}_{\mathrm{nt}}\| - \|\overline{M}_{\mathrm{nt}}\|)\partial\tilde{w} \rangle_i \tag{12}$$

where the notation $\langle\cdot\rangle_i$ indicates the value of the function at the ith corner point. The vanishing of $\partial\Pi$, for arbitrary variations ∂w in Ω, $\partial\tilde{\mathbf{t}}$ on Γ and $\partial\tilde{\mathbf{u}}$ on Γ_2, gives the following set of Euler equations

$$\mathscr{D}^{\mathrm{T}}\mathbf{E}\mathscr{D}w - q + \rho h\ddot{w} = 0 \quad \text{in } \Omega \tag{13}$$

$$\tilde{\mathbf{u}} = \mathbf{u} \quad \text{on } \Gamma \tag{14}$$

$$\tilde{\mathbf{t}} = \mathbf{t} \quad \text{on } \Gamma \tag{15}$$

$$\tilde{\mathbf{t}} = \bar{\mathbf{t}} \quad \text{on } \Gamma_2 \tag{16}$$

$$\|\tilde{M}_{\mathrm{nt}}\|_i = \|M_{\mathrm{nt}}\|_i \quad i = 1, \ldots, \mathrm{NC} \tag{17}$$

$$\|M_{\mathrm{nt}}\|_i = \|\overline{M}_{\mathrm{nt}}\|_i \quad i = 1, \ldots, \mathrm{NC}_2 \tag{18}$$

Consequently, assuming that the compatibility equations (1) and the constitutive equations (4) are verified and the boundary conditions (6) are identically satisfied, the solution of the plate problem is given in terms of the functions w, $\tilde{\mathbf{u}}$ and $\tilde{\mathbf{t}}$ which make Π stationary.

4. Functional discretization and plate dynamics model

In order to obtain a meshfree model for the plate dynamic problem by using the variational principle previously described, consider a set of N nodes randomly chosen in which a part of those, namely N_{B}, lies on the plate boundary Γ whereas the other N_{D} belong to the plate domain Ω (see Fig. 2). The domain displacement field w, describing the plate flexural behavior, is approximated by means of a linear combination of time independent trial functions w_i^*. The number of trial function employed for the approximation of the plate deflection is linked to the degrees of freedom introduced by the nodes, explicitly the

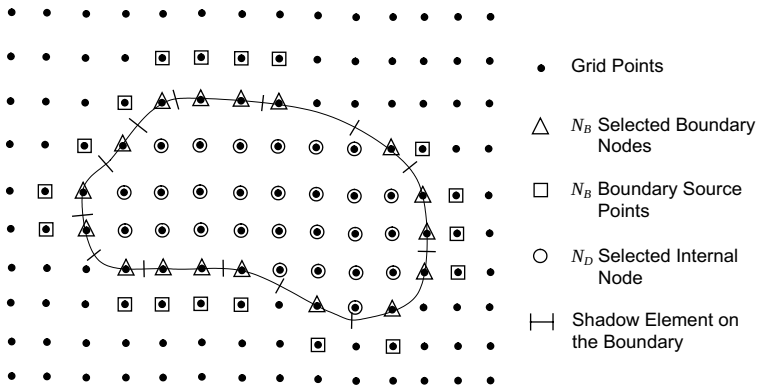

Fig. 2. Discretization scheme.

deflection for the N_D domain nodes and the deflection and normal slope for the N_B nodes belonging to the plate boundary. Then, one has

$$w = \sum_{i=1}^{2N_B+N_D} w_i^* s_i = \mathbf{W}^* \mathbf{s} \tag{19}$$

where $\mathbf{s}$ is the vector of the unknown time dependent coefficients $s_i = s_i(t)$ and $\mathbf{W}^*$ is the matrix of the trial functions w_i^*. The trial functions w_i^* can be thought as the solutions in an infinite anisotropic plate corresponding to a static load q_i^* and thus, these solutions associated with the solutions in an infinite domain of the equation

$$\mathscr{D}^T \mathbf{E} \mathscr{D} w_i^* = q_i^*(x_1, x_2) \tag{20}$$

With this assumption, the generalized displacements on the boundary Γ can be expressed in terms of trial functions as

$$\mathbf{u} = \begin{bmatrix} w \\ -\partial w/\partial n \end{bmatrix} = \begin{bmatrix} \mathbf{W}^* \\ -\partial \mathbf{W}^*/\partial n \end{bmatrix} \mathbf{s} = \mathbf{U}^* \mathbf{s} \tag{21}$$

On the other hand, the boundary generalized displacement and traction variables are expressed as

$$\tilde{\mathbf{u}} = \begin{bmatrix} w \\ -\frac{\partial w}{\partial n} \end{bmatrix} = \begin{bmatrix} \mathbf{N}_{w1} & \mathbf{N}_{w2} \\ \mathbf{N}_{\varphi 1} & \mathbf{N}_{\varphi 2} \end{bmatrix} \begin{bmatrix} \boldsymbol{\delta}_1 \\ \boldsymbol{\delta}_2 \end{bmatrix} = \begin{bmatrix} \mathbf{N}_1 & \mathbf{N}_2 \end{bmatrix} \begin{bmatrix} \boldsymbol{\delta}_1 \\ \boldsymbol{\delta}_2 \end{bmatrix} = \mathbf{N}\boldsymbol{\delta} \tag{22}$$

$$\tilde{\mathbf{t}} = \begin{bmatrix} \tilde{T}_{eq} \\ \tilde{M}_n \end{bmatrix} = \boldsymbol{\Psi} \mathbf{p} \tag{23}$$

where $\boldsymbol{\delta}$ is the vector of the generalized displacements associated with the N nodes of the discretization, $\mathbf{p}$ is the vector of the nodal generalized tractions associated with the N_B boundary nodes and $\mathbf{N}$ and $\boldsymbol{\Psi}$ are matrices of interpolants whose functional dependencies will be determined later. The subscripts 1 and 2 refer to constrained and free nodal displacements, respectively. By substituting these approximations for w, $\tilde{\mathbf{u}}$, and $\tilde{\mathbf{t}}$ into Eq. (11), the expression of the discretized functional Π for the plate is obtained. After integrating by parts, the stationarity conditions of Π with respect to the discrete independent variables $\mathbf{s}$, $\boldsymbol{\delta}_2$ and $\mathbf{p}$ yield the following set of equations

$$\left(\int_\Gamma \mathbf{U}^{*T} \mathbf{P}^* \, d\Gamma - \sum_{i=1}^{NC} \langle \mathbf{W}^{*T} \| \mathbf{M}_{nt}^* \| \rangle_i + \int_\Omega \mathbf{W}^{*T} \mathbf{Q}^* \, d\Omega \right) \mathbf{s} + \rho h \int_\Omega \mathbf{W}^{*T} \mathbf{W}^* \, d\Omega \ddot{\mathbf{s}} - \int_\Omega \mathbf{W}^{*T} q \, d\Omega$$
$$- \int_\Gamma \mathbf{U}^{*T} \boldsymbol{\Psi} \, d\Gamma \mathbf{p} + \sum_{i=1}^{NC} \langle \mathbf{W}^{*T} \| \tilde{M}_{nt} \| \rangle_i = \mathbf{0} \tag{24}$$

$$\int_\Gamma \mathbf{N}_2^T \boldsymbol{\Psi} \, d\Gamma \mathbf{p} - \int_{\Gamma_2} \mathbf{N}_2^T \bar{\mathbf{t}} \, d\Gamma + \sum_{i=1}^{NC_2} \langle \mathbf{N}_{w2}^T \| \overline{M}_{nt} \| \rangle_i - \sum_{i=1}^{NC} \langle \mathbf{N}_{w2}^T \| \tilde{M}_{nt} \| \rangle_i = \mathbf{0} \tag{25}$$

$$\int_\Gamma \boldsymbol{\Psi}^T \mathbf{U}^* \, d\Gamma \mathbf{s} - \int_\Gamma \boldsymbol{\Psi}^T \mathbf{N} \, d\Gamma \boldsymbol{\delta} = \mathbf{0} \tag{26}$$

where $\mathbf{P}^*$ is the matrix of the boundary generalized tractions associated with the trial functions w_i^* whereas the vector $\mathbf{Q}^*$ contains the relative loads q_i^*. Eq. (26) can be satisfied independently from the choice of the interpolant matrix $\boldsymbol{\Psi}$ if it results

$$\mathbf{U}^* \mathbf{s} = \mathbf{N}\boldsymbol{\delta} \quad \text{on } \Gamma \tag{27}$$

At this point, the relation between the coefficient vector $\mathbf{s}$ and the displacements of the points chosen for the discretization process, i.e. the nodal displacements, can be established. Evaluating Eq. (27) at the nodal points lying on the plate boundary, by virtue of the properties of the interpolants, one obtains the relationships between $\mathbf{s}$ and the generalized displacements $\boldsymbol{\delta}_\Gamma$ of the boundary nodes

$$\overline{\mathbf{U}}^*\mathbf{s} = \boldsymbol{\delta}_\Gamma \tag{28}$$

where the elements of the matrix $\overline{\mathbf{U}}^*$ are the values of the functional matrix $\mathbf{U}^*$ computed at the boundary nodes. In a similar way, collocating Eq. (19) at the internal nodes, a second set of relationships can be established and it gives

$$\overline{\mathbf{W}}^*\mathbf{s} = \boldsymbol{\delta}_\Omega \tag{29}$$

In Eq. (29) the elements of the matrix $\overline{\mathbf{W}}^*$ are the values of $\mathbf{W}^*$ calculated at the internal nodes and $\boldsymbol{\delta}_\Omega$ is the vector collecting the displacements of the domain nodes. If the trial functions are chosen so as to be regular and linearly independent, then the matrix

$$\boldsymbol{\Lambda} = \begin{bmatrix} \overline{\mathbf{U}}^* \\ \overline{\mathbf{W}}^* \end{bmatrix} \tag{30}$$

is square and possesses an inverse $\boldsymbol{\Phi} = \boldsymbol{\Lambda}^{-1}$. Therefore from Eqs. (28) and (29) one has

$$\mathbf{s} = \boldsymbol{\Lambda}^{-1}\begin{bmatrix} \boldsymbol{\delta}_\Gamma \\ \boldsymbol{\delta}_\Omega \end{bmatrix} = \boldsymbol{\Phi}\begin{bmatrix} \boldsymbol{\delta}_\Gamma \\ \boldsymbol{\delta}_\Omega \end{bmatrix} = [\,\boldsymbol{\Phi}_\Gamma \quad \boldsymbol{\Phi}_\Omega\,]\begin{bmatrix} \boldsymbol{\delta}_\Gamma \\ \boldsymbol{\delta}_\Omega \end{bmatrix} = [\,\boldsymbol{\Phi}_1 \quad \boldsymbol{\Phi}_2\,]\begin{bmatrix} \boldsymbol{\delta}_1 \\ \boldsymbol{\delta}_2 \end{bmatrix} \tag{31}$$

Eqs. (27) and (31) imply the following functional expression of the interpolant matrix $\mathbf{N}$ in terms of trial functions

$$\mathbf{N} = \mathbf{U}^*\boldsymbol{\Lambda}^{-1} = \mathbf{U}^*\boldsymbol{\Phi} = \begin{bmatrix} \mathbf{W}^* \\ -\frac{\partial \mathbf{W}^*}{\partial n} \end{bmatrix}[\,\boldsymbol{\Phi}_1 \quad \boldsymbol{\Phi}_2\,] = \begin{bmatrix} \mathbf{N}_{w1} & \mathbf{N}_{w2} \\ \mathbf{N}_{\varphi 1} & \mathbf{N}_{\varphi 2} \end{bmatrix} \tag{32}$$

Pre-multiplying Eq. (24) by $\boldsymbol{\Phi}_2^{\mathrm{T}}$, by using Eqs. (25) and (31), and defining the stiffness matrix $\mathbf{K}$ and the mass matrix $\mathbf{M}$ as

$$\mathbf{K} = \boldsymbol{\Phi}_2^{\mathrm{T}}\left(\int_\Gamma \mathbf{U}^{*\mathrm{T}}\mathbf{P}^*\,\mathrm{d}\Gamma - \sum_{i=1}^{\mathrm{NC}}\langle \mathbf{W}^{*\mathrm{T}}\|\mathbf{M}^*_{\mathrm{nt}}\|\rangle_i + \int_\Omega \mathbf{W}^{*\mathrm{T}}\mathbf{Q}^*\,\mathrm{d}\Omega\right)\boldsymbol{\Phi}_2 = \boldsymbol{\Phi}_2^{\mathrm{T}}\overline{\mathbf{K}}\boldsymbol{\Phi}_2 \tag{33}$$

$$\mathbf{M} = \rho h\boldsymbol{\Phi}_2^{\mathrm{T}}\int_\Omega \mathbf{W}^{*\mathrm{T}}\mathbf{W}^*\,\mathrm{d}\Omega\boldsymbol{\Phi}_2 = \boldsymbol{\Phi}_2^{\mathrm{T}}\overline{\mathbf{M}}\boldsymbol{\Phi}_2 \tag{34}$$

one obtains the plate dynamic model

$$\mathbf{M}\ddot{\boldsymbol{\delta}}_2 + \mathbf{K}\boldsymbol{\delta}_2 = \int_{\Gamma_2}\mathbf{N}_2^{\mathrm{T}}\bar{\mathbf{t}}\,\mathrm{d}\Gamma + \int_\Omega \mathbf{N}_{w2}^{\mathrm{T}}q\,\mathrm{d}\Omega - \sum_{i=1}^{\mathrm{NC}_2}\langle \mathbf{N}_{w2}^{\mathrm{T}}\|\overline{M}_{\mathrm{nt}}\|\rangle_i - \boldsymbol{\Phi}_2^{\mathrm{T}}\overline{\mathbf{M}}\boldsymbol{\Phi}_1\ddot{\boldsymbol{\delta}}_1 - \boldsymbol{\Phi}_2^{\mathrm{T}}\overline{\mathbf{K}}\boldsymbol{\Phi}_1\boldsymbol{\delta}_1 \tag{35}$$

The present approach leads to a meshfree model as suggested by the structure of the resolving system obtained. Indeed, the model proposed involves only the displacements of the nodal points introduced by the discretization process of the functional, whereas the influence matrices, i.e. the stiffness and mass matrix, are defined in terms of the trial functions. Their construction does not call for assembly procedures based on a mesh definition. Moreover, the proposed approach evidences some interesting features pointed out in the following. Due to the kind of trial functions employed, the matrices $\mathbf{K}$ and $\mathbf{M}$ are frequency-independent. They are symmetric and positive definite (Davì and Milazzo, 1997b; Davì et al., 1997) and then these two fundamental properties of the continuum, namely symmetry and definiteness of the structural operators, are preserved with the related theoretical and computational advantages.

5. Displacement boundary method

The analysis of the discretization process and of the resulting model clearly indicates that the effectiveness of the proposed approach is strictly correlated to the trial functions employed. In the boundary models based on the proposed formulation (Davì and Milazzo, 1994, 1997b), the trial functions have been chosen to be the static fundamental solutions in an infinite isotropic domain corresponding to point loads. Accordingly, also in the present approach, the w_i^* have been chosen to be the static fundamental solutions in an infinite anisotropic plate corresponding to a point load and a point couple with magnitude c_i^*, applied at the location P_i which is referred as the source point. Explicitly, the fundamental solution due to a point load corresponds to the solution of the Eq. (20) for a load q_i^* defined as

$$q_i^* = c_i^* \delta(P - P_i) \tag{36}$$

where $\delta(P - P_i)$ denotes the Dirac's function. The fundamental solution due to a point couple about an axis orthogonal to the boundary outer normal n can be directly obtained applying the operator $\partial/\partial n$ to the fundamental solution for the point load. These trial functions, namely the anisotropic plate fundamental solutions, can be associated with the source points and so they become very well-suited for the meshfree discretization process. In particular, according to Eq. (21), for the boundary nodes where there are two unknown nodal generalized displacements, namely the nodal deflection and normal slope, both the fundamental solutions are defined with the same source point. On the other hand, at the internal nodes only the fundamental solution due to a point load is considered as the nodal deflection is the sole unknown in accordance with Eq. (19). The fundamental solutions are correlated to the nodal points basing on the following criterion: for the fundamental solutions carried by the internal nodes the source point is chosen coincident with the node whereas the source point of the fundamental solutions associated with boundary nodal points is located outside the domain along the boundary outer normal at the node. This selection of the fundamental solutions as trial functions leads to the DBM (Davì and Milazzo, 1997b) that can be classified as a meshfree method with very appealing features. In fact, by employing the problem fundamental solutions and remembering the properties of integrals involving Dirac functions, the domain integral in the stiffness matrix definition (Eq. (33)) can be directly evaluated and the calculation of the stiffness matrix requires only boundary integrations. Moreover, due to the choice of the source points, which do not lie on the plate boundary, the kernels involve only non-singular functions having advantages in computation consequently. The other domain integral that appears in the definition of the mass matrix $\mathbf{M}$ can be properly transformed so as to obtain a pure boundary model of the discretized plate. To this purpose, consider a particular solution of the equation

$$\mathscr{D}^{\mathrm{T}}\mathbf{E}\mathscr{D}f_j^* = \boldsymbol{\Theta}^{\mathrm{T}}\boldsymbol{\Xi}^{\mathrm{T}}\mathbf{E}\boldsymbol{\Xi}\boldsymbol{\Theta}f_j^* = w_j^* \quad \text{in } \Omega \tag{37}$$

where w_j^* is the jth fundamental solution. The functions f_j^* are called companion solutions and they are collected in the vector $\mathbf{F}$. By applying the reciprocity theorem to the companion solution vector $\mathbf{F}$ and to the fundamental solution vector $\mathbf{W}^*$, the matrix $\overline{\mathbf{M}}$ can be expressed as

$$\begin{aligned}\frac{1}{\rho h}\overline{\mathbf{M}} &= \int_\Omega \mathbf{W}^{*\mathrm{T}}\mathbf{W}^*\,\mathrm{d}\Omega = \int_\Omega \mathbf{W}^{*\mathrm{T}}\boldsymbol{\Theta}^{\mathrm{T}}\boldsymbol{\Xi}^{\mathrm{T}}\mathbf{E}\boldsymbol{\Xi}\boldsymbol{\Theta}\mathbf{F}\,\mathrm{d}\Omega \\ &= \int_\Gamma [\mathbf{W}^{*\mathrm{T}}\boldsymbol{\Theta}_n^{\mathrm{T}}\boldsymbol{\Xi}^{\mathrm{T}}\mathbf{E}\boldsymbol{\Xi}\boldsymbol{\Theta}\mathbf{F} - (\boldsymbol{\Theta}\mathbf{W}^*)^{\mathrm{T}}\boldsymbol{\Xi}_n^{\mathrm{T}}\mathbf{E}\boldsymbol{\Xi}\boldsymbol{\Theta}\mathbf{F}]\,\mathrm{d}\Gamma + \int_\Gamma [(\boldsymbol{\Xi}_n^{\mathrm{T}}\mathbf{E}\boldsymbol{\Xi}\boldsymbol{\Theta}\mathbf{W}^*)^{\mathrm{T}}\boldsymbol{\Theta}\mathbf{F} \\ &\quad - (\boldsymbol{\Theta}_n^{\mathrm{T}}\boldsymbol{\Xi}^{\mathrm{T}}\mathbf{E}\boldsymbol{\Xi}\boldsymbol{\Theta}\mathbf{W}^*)^{\mathrm{T}}\mathbf{F}]\,\mathrm{d}\Gamma + \int_\Omega \mathbf{Q}^{*\mathrm{T}}\mathbf{F}\,\mathrm{d}\Omega\end{aligned} \tag{38}$$

where the operators $\boldsymbol{\Theta}_n^{\mathrm{T}}$ and $\boldsymbol{\Xi}_n^{\mathrm{T}}$ are obtained from $\boldsymbol{\Theta}$ and $\boldsymbol{\Xi}$ by substituting the derivatives with the corresponding direction cosines of the boundary outer normal. Eq. (38), taking again the Dirac's function

properties into account for the evaluation of the domain integral on the right-hand side, allows one to express the mass matrix in terms of boundary integrals. Performing the transformation above-described, both the mass matrix and the stiffness matrix can be calculated through integration of regular kernels on the boundary only, thus reducing the problem dimensionality and recovering a boundary character for the approach. In conclusion, the dynamic model obtained for anisotropic plate is constituted by a set of linear differential equations that exhibits the same features of the most common finite element dynamic resolving systems, namely symmetry and definiteness. Therefore, for the numerical solution, the present DBM allows the application of the standard procedures available for finite element models coupled with a meshfree nature and boundary element computational advantages.

6. Fundamental and companion solutions

The anisotropic plate fundamental solutions due to point load and couple are an essential part of the proposed method. Fundamental solutions for anisotropic plates make use of complex variable theory according to Lekhnitskii (1968) and they have been presented by Suchar (1964) and Mossakowski (1995). Here, the attention is focused on the point load fundamental solution because the point couple fundamental solution follows from the former by proper differentiation with respect to the couple axis direction. The considered fundamental solution is governed by the following equilibrium equation

$$\mathscr{D}^{\mathrm{T}}\mathbf{E}\mathscr{D}w_i^* = c_i^*\delta(P-P_i) \tag{39}$$

with the known meaning of the symbols. Observing that Eq. (39) is a homogeneous equation, except that at the point P_i where the solution is singular, it admits particular solutions of the form

$$w = \frac{1}{2}\alpha(X_1+\mu X_2)^2\left[\ln(X_1+\mu X_2)-\frac{3}{2}\right] \tag{40}$$

where μ and λ are complex constants to be determined and

$$X_k = x_k(P)-x_k(P_i) \quad (k=1,2) \tag{41}$$

Substitution of Eq. (40) into Eq. (39) leads to the eigenvalue problem corresponding to the following characteristic equation

$$\begin{aligned}&\boldsymbol{\Theta}_2^{\mathrm{T}}\boldsymbol{\Xi}_2^{\mathrm{T}}\mathbf{E}\boldsymbol{\Xi}_2\boldsymbol{\Theta}_2\mu^4 + 2(\boldsymbol{\Theta}_1^{\mathrm{T}}\boldsymbol{\Xi}_2^{\mathrm{T}}\mathbf{E}\boldsymbol{\Xi}_2\boldsymbol{\Theta}_2 + \boldsymbol{\Theta}_2^{\mathrm{T}}\boldsymbol{\Xi}_1^{\mathrm{T}}\mathbf{E}\boldsymbol{\Xi}_2\boldsymbol{\Theta}_2)\mu^3 + (2\boldsymbol{\Theta}_1^{\mathrm{T}}\boldsymbol{\Xi}_1^{\mathrm{T}}\mathbf{E}\boldsymbol{\Xi}_2\boldsymbol{\Theta}_2 + 2\boldsymbol{\Theta}_1^{\mathrm{T}}\boldsymbol{\Xi}_2^{\mathrm{T}}\mathbf{E}\boldsymbol{\Xi}_1\boldsymbol{\Theta}_2 + \boldsymbol{\Theta}_1^{\mathrm{T}}\boldsymbol{\Xi}_2^{\mathrm{T}}\mathbf{E}\boldsymbol{\Xi}_2\boldsymbol{\Theta}_1\\ &\quad + \boldsymbol{\Theta}_2^{\mathrm{T}}\boldsymbol{\Xi}_1^{\mathrm{T}}\mathbf{E}\boldsymbol{\Xi}_1\boldsymbol{\Theta}_2)\mu^2 + 2(\boldsymbol{\Theta}_1^{\mathrm{T}}\boldsymbol{\Xi}_2^{\mathrm{T}}\mathbf{E}\boldsymbol{\Xi}_1\boldsymbol{\Theta}_1 + \boldsymbol{\Theta}_2^{\mathrm{T}}\boldsymbol{\Xi}_1^{\mathrm{T}}\mathbf{E}\boldsymbol{\Xi}_1\boldsymbol{\Theta}_1)\mu + \boldsymbol{\Theta}_1^{\mathrm{T}}\boldsymbol{\Xi}_1^{\mathrm{T}}\mathbf{E}\boldsymbol{\Xi}_1\boldsymbol{\Theta}_1 = 0\end{aligned} \tag{42}$$

where the matrices $\boldsymbol{\Theta}_m$ and $\boldsymbol{\Xi}_m$ $(m=1,2)$ are obtained from the operators $\boldsymbol{\Theta}$ and $\boldsymbol{\Xi}$ by setting the derivative with respect to x_m equal to one and replacing all the other terms with zeros. The solution of Eq. (42) gives four eigenvalues μ_k that form conjugate pairs (Lekhnitskii, 1968). In the case of distinct eigenvalues, the fundamental solutions are obtained by superposing four solutions of the form (40), associated with the eigenvalues μ_k and one has

$$w_i^* = \sum_{k=1}^{4}\frac{1}{2}\alpha_{ik}^*(X_1+\mu_k X_2)^2\left[\ln(X_1+\mu_k X_2)-\frac{3}{2}\right] \tag{43}$$

Without loss of generality, assuming that $\mathrm{Im}[\mu_k]>0$ for $k=1,2$, the deflection of the fundamental solution can be also written as (LaMattina et al., 1998)

$$w_i^* = \sum_{k=1}^{2}\mathrm{Re}\left[\alpha_{ik}^*(X_1+\mu_k X_2)^2\left\{\ln(X_1+\mu_k X_2)-\frac{3}{2}\right\}\right] \tag{44}$$

In the case of multiple eigenvalues of Eq. (42), the material is called degenerate and the fundamental solutions have different expressions depending on the eigenvalue order. The discussion of this case is out of the scope of the present paper and the reader is referred to Lekhnitskii (1968) for the analysis of this topic. The complex constants α^*_{ik} are determined by enforcing the compatibility conditions, which recover the single-value character of the deflection and of its x_2-direction derivatives, and the equilibrium condition at the source point. The vector $\boldsymbol{\alpha}^*_i$ collecting the coefficients α^*_{ik} is then computed by

$$\boldsymbol{\alpha}^*_i = \begin{bmatrix} \alpha_{i1} \\ \alpha_{i2} \\ \alpha_{i3} \\ \alpha_{i4} \end{bmatrix} = \begin{bmatrix} 1 & 1 & -1 & -1 \\ \mu_1 & \mu_2 & -\hat{\mu}_1 & -\hat{\mu}_2 \\ \mu_1^2 & \mu_2^2 & -\hat{\mu}_1^2 & -\hat{\mu}_2^2 \\ \eta_1 & \eta_2 & \hat{\eta}_1 & \hat{\eta}_2 \end{bmatrix}^{-1} \begin{bmatrix} 0 \\ 0 \\ 0 \\ c^*_i \end{bmatrix} \tag{45}$$

where the hat denotes the complex conjugate. In the previous expression, one has to set

$$\eta_k = \frac{2\pi}{1+\mu_k^2} \overline{\boldsymbol{\Theta}}_k^{\mathrm{T}} \overline{\boldsymbol{\Xi}}_k^{\mathrm{T}} \mathbf{E} \overline{\boldsymbol{\Xi}} \begin{bmatrix} 1 - \sqrt{-1}\mu_k \\ \mu_k + \sqrt{-1} \end{bmatrix} \tag{46}$$

where the matrices $\overline{\boldsymbol{\Theta}}_k$ and $\overline{\boldsymbol{\Xi}}_k$ are obtained from the operators $\boldsymbol{\Theta}$ and $\boldsymbol{\Xi}$ by replacing the derivatives with respect to x_1 with one and the derivatives with respect to x_2 with μ_k. It is worth to note that the present fundamental solution has been derived using a suitable matrix notation, which is very advantageous for computer implementation. According to the form of the fundamental solution given by Eq. (44) the corresponding companion solution can be expressed as

$$f^*_i = 2 \sum_{k=1}^{2} \mathrm{Re}[\zeta_k(X_1, X_2)] \tag{47}$$

where the functions $\zeta_k(X_1, X_2)$ are particular solutions of the following equation

$$\mathscr{D}^{\mathrm{T}} \mathbf{E} \mathscr{D} \zeta_k = \frac{1}{2} \alpha^*_{ik} (X_1 + \mu_k X_2)^2 \left[\ln(X_1 + \mu_k X_2) - \frac{3}{2} \right] \tag{48}$$

By defining the complex variables

$$Z_k = X_1 + \mu_k X_2 \quad k = 1, 2 \tag{49}$$

the Eq. (48) can be reduced to a set of two equations that are

$$(\mu_k - \hat{\mu}_k)^2 \sqrt{D_{22}} \frac{\partial^2 \xi_k(Z_k, \widehat{Z}_k)}{\partial Z_k \partial \widehat{Z}_k} = -\frac{1}{2} \alpha^*_{ik} Z_k^2 \left(\ln Z_k - \frac{3}{2} \right) \tag{50}$$

$$(\mu_{k-(-1)^k} - \hat{\mu}_{k-(-1)^k})^2 \sqrt{D_{22}} \frac{\partial^2 \zeta_k(Z_{k-(-1)^k}, \widehat{Z}_{k-(-1)^k})}{\partial Z_{k-(-1)^k} \partial \widehat{Z}_{k-(-1)^k}} = -\tilde{\xi}_k(Z_{k-(-1)^k}, \widehat{Z}_{k-(-1)^k}) \tag{51}$$

where the function $\tilde{\xi}_k$ is obtained from ξ_k by expressing the variables Z_k and $\widehat{Z}_k$ in terms of $Z_{k-(-1)^k}$ and $\widehat{Z}_{k-(-1)^k}$ by means of the following relationship

$$\begin{bmatrix} Z_k \\ \widehat{Z}_k \end{bmatrix} = \frac{1}{\mu_{k-(-1)^k} - \hat{\mu}_{k-(-1)^k}} \begin{bmatrix} \mu_k - \hat{\mu}_{k-(-1)^k} & \mu_{k-(-1)^k} - \mu_k \\ \hat{\mu}_k - \hat{\mu}_{k-(-1)^k} & \mu_{k-(-1)^k} - \hat{\mu}_k \end{bmatrix} \begin{bmatrix} Z_{k-(-1)^k} \\ \widehat{Z}_{k-(-1)^k} \end{bmatrix} = \mathbf{A}^k \begin{bmatrix} Z_{k-(-1)^k} \\ \widehat{Z}_{k-(-1)^k} \end{bmatrix} \tag{52}$$

The Eqs. (50) and (51) can be sequentially integrated and employing Eq. (52) they provide the following expression of the companion functions ζ_k

$$\zeta_k = \frac{1}{720D_{22}[A^k_{11}A^k_{12}(\mu_k - \hat{\mu}_k)(\mu_{k-(-1)^k} - \hat{\mu}_{k-(-1)^k})]^2}\left[(A^k_{11}A^k_{22} + A^k_{12}A^k_{21})Z^6_k\left(\frac{49}{20} - \ln Z_k\right)\right.$$
$$\left. - A^k_{11}A^k_{12}Z^5_k\widehat{Z}_k\left(\frac{137}{10} - 6\ln Z_k\right)\right] + \beta_k Z^6_k \ln Z_k \tag{53}$$

where the coefficients A^k_{mn} are the elements of the matrix $\mathbf{A}^k$. It is worth to note that, according to complex function theory, the last term of Eq. (53) satisfies the homogeneous form of the problem governing equation and it is added to ensure the regularity of the kernel involved in the mass matrix. For this purpose, the coefficients β_k are determined by enforcing the continuity of the companion solution and its derivatives up to the third order on the Gauss plane.

7. Numerical examples and discussion

The present method is examined by applying the formulation to the analysis of anisotropic plates free vibration, which is a fundamental issue of dynamic analysis. A computer code has been developed to implement the formulation proposed, which follows these basic features: (i) The plate geometry, boundary conditions and discretization are given in terms of boundary and domain nodes and to each node the corresponding source point is associated (see Fig. 2). For the domain nodes, the source point matches the node; the source points associated with the boundary nodes are obtained by locating the fundamental solution source point outside the domain along the boundary outer normal at the nodal point. According with Davì and Milazzo (1994), the ratio between the distance of the source point from the nodal point and the distance between contiguous boundary nodes is chosen equal to 1. (ii) The generalized elasticity matrix is computed and the fundamental and companion solutions are determined through Eqs. (44) and (47) after the eigenvalue problem given by Eq. (42) was solved. (iii) The matrix $\mathbf{\Phi}$ is computed by applying the collocation procedure described in Eqs. (28) and (29); according to Eq. (31), the matrix $\mathbf{\Phi}$ is suitably partitioned taking the boundary conditions into account. (iv) According to Eqs. (33) and (38), the influence matrices $\overline{\mathbf{K}}$ and $\overline{\mathbf{M}}$ are computed performing the required boundary integrations and calculating the residual domain integrals by using the Dirac's function properties. The boundary integrations are numerically

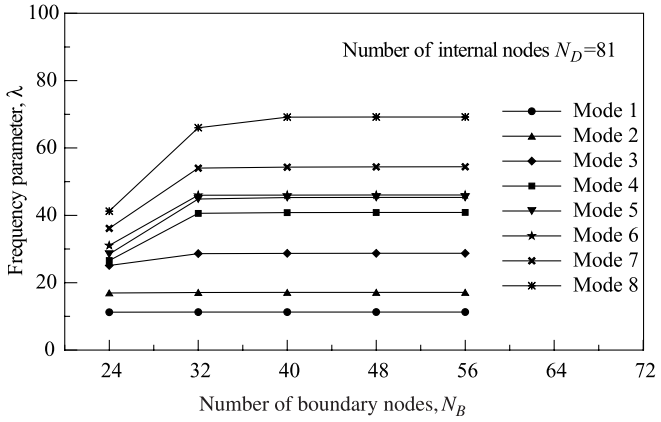

Fig. 3. Convergence pattern of λ vs. N_B for the $\vartheta = 0°$ simply-supported plate with $N_D = 81$.

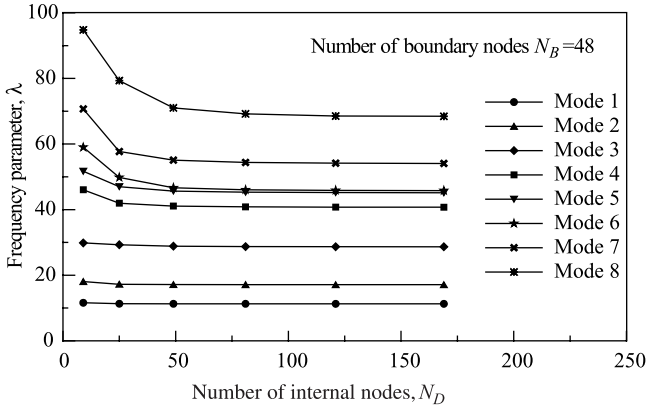

Fig. 4. Convergence pattern of λ vs. N_D for the $\vartheta = 0°$ simply-supported plate with $N_B = 48$.

Table 1
Free vibration frequency parameter λ of $[\vartheta°/-\vartheta°/\vartheta°/-\vartheta°/\vartheta°]$ angle-ply, simply-supported square plates

	Mode[a]	ϑ			
		0°	15°	30°	45°
$[\vartheta°/-\vartheta°/\vartheta°/-\vartheta°/\vartheta°]$	1	11.283	11.832	12.913	13.439
		(11.29)	(11.89)	(13.10)	(13.70)
		[11.30]	[11.82]	[12.98]	[13.61]
		11.288			
	2	17.119	19.707	25.090	28.781
		(17.13)	(19.82)	(25.36)	(28.94)
		[17.13]	[19.76]	[25.21]	[28.75]
		17.125			
	3	28.689	32.985	36.842	34.282
		(28.69)	(33.10)	(37.15)	(34.92)
		[28.70]	[32.93]	[36.97]	[34.68]
		28.683			
	4	40.761	39.665	42.902	48.953
		(40.74)	(39.71)	(43.13)	(49.29)
		[40.77]	[39.53]	[42.65]	[48.90]
		40.739			
	5	45.183	47.396	52.500	59.551
		(45.16)	(47.58)	(53.18)	(59.73)
		[45.18]	[47.42]	[52.83]	[59.25]
		45.150			
	6	45.839	51.439	65.698	64.626
		(45.78)	(51.48)	(65.97)	(65.78)
		[46.23]	[52.73]	[66.48]	[65.34]
		45.774			
	7	54.138	60.828	75.647	74.127
		(54.08)	(61.09)	(75.87)	(74.56)
		[54.98]	[61.11]	[75.76]	[74.28]
		54.065			
	8	68.403	74.048	76.029	87.860
		(68.14)	(73.95)	(76.57)	(88.41)
		[69.64]	[74.08]	[77.65]	[88.86]
		68.134			

[a] The values in parentheses are adapted from Leissa and Narita (1989). The values in square brackets are adapted from Chow et al. (1992). The values in italic are adapted from Vasiliev (1993).

performed on shadow elements set on the plate boundary (see Fig. 2) by using standard 12-point Gaussian quadrature. (v) Finally, the stiffness and mass matrices are computed and the dynamic model, namely Eq. (35), is solved by standard numerical procedures for eigenvalue computation. By using the computer code, graphite/epoxy plates have been analyzed to establish the applicability and effectiveness of the proposed approach. The following properties have been adopted for the graphite/epoxy composite

$$E_L/E_T = 15.4, \quad G_{LT}/E_T = 0.79, \quad v_{LT} = 0.30$$

where E_L is the Young's modulus in the direction parallel to the fibers, while E_T is the one orthogonal to the fiber direction; G_{LT} is the shear modulus in the lamina plane and v_{LT} is the major Poisson's ratio. To demonstrate the soundness of the DBM for anisotropic plates, accuracy and convergence studies have been carried out. Convergence analyses have been performed for square plates with side length a, thickness h and $[\vartheta°/-\vartheta°/\vartheta°/-\vartheta°/\vartheta°]$ layup. To investigate the effect of the degree of anisotropy on the solution accuracy, different values of ϑ have been considered and in particular ϑ has been taken as 0°, 15°, 30° and 45°. All of the plates have been analyzed for both simply-supported and clamped edge conditions on all four edges so as to highlight the effect of the boundary conditions on the method effectiveness. The computations show the fundamental convergence characteristics described in the following in terms of the frequency parameter

$$\lambda = \omega a^2 \sqrt{\frac{12\rho(1 - v_{LT}v_{TL})}{E_L h^2}} \tag{54}$$

Table 2
Free vibration frequency parameter λ of $[\vartheta°/-\vartheta°/\vartheta°/\text{-}\vartheta°/\vartheta°]$ angle-ply, square plates with clamped edges

	Mode[a]	ϑ			
		0°	15°	30°	45°
$[\vartheta°/-\vartheta°/\vartheta°/-\vartheta°/\vartheta°]$ 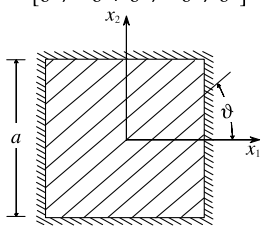	1	23.717	23.452	22.772	22.429
		(23.86)	(23.46)	(22.72)	(22.40)
		[23.852]	[23.453]	[22.713]	[22.381]
	2	29.599	31.513	36.659	41.754
		(29.71)	(31.48)	(36.54)	(41.64)
		[29.715]	[31.479]	[36.546]	[41.465]
	3	41.672	45.889	54.263	48.498
		(41.73)	(45.80)	(54.02)	(48.32)
		[41.721]	[45.790]	[54.012]	[48.316]
	4	60.241	60.579	57.369	65.370
		(60.24)	(60.38)	(57.17)	(65.09)
		[60.229]	[60.383]	[57.156]	[65.086]
	5	62.895	66.333	70.551	78.094
		(62.93)	(66.47)	(70.09)	(77.76)
		[62.974]	[66.374]	[70.079]	[77.746]
	6	67.432	68.316	83.646	84.591
		(67.45)	(67.96)	(83.37)	(84.06)
		[67.462]	[67.977]	[83.369]	[84.037]
	7	76.536	81.930	95.811	94.299
		(76.46)	(81.36)	(95.27)	(93.58)
		[76.448]	[81.399]	[95.269]	[93.696]
	8	84.446	91.963	101.18	109.89
		(85.06)	(92.42)	(100.4)	(109.00)
		[85.051]	[92.375]	(100.37)	[109.14]

[a] The values in parentheses are adapted from Chow et al. (1992). The values in square brackets are adapted from Han and Petyt (1996).

where ω is the natural angular frequency. The convergence properties are not influenced from the degree of anisotropy and from the position of the source points associated with the boundary nodes. For a fixed number of internal nodes (N_D = constant) the convergence with respect to the number of boundary nodes N_B is monotonic, from below for all of the vibration modes. An example of this convergence pattern is given in Fig. 3 for the $\vartheta = 0°$ simply-supported plate. Similar convergence patterns were obtained for different number of internal points, for different stacking sequences and for different boundary conditions. For a fixed number of boundary nodes (N_B = constant) the convergence with respect to the number of internal nodes N_D is monotonic, from above for all of the vibration modes. An example of this convergence pattern is given in Fig. 4 for the $\vartheta = 0°$ simply-supported plate. Similar convergence patterns have been also obtained for different number of internal points, for different stacking sequences and for different boundary conditions. The examination of the convergence behavior above-described lead to the following considerations. The rate of convergence and the accuracy of the proposed approach depend on the ratio between

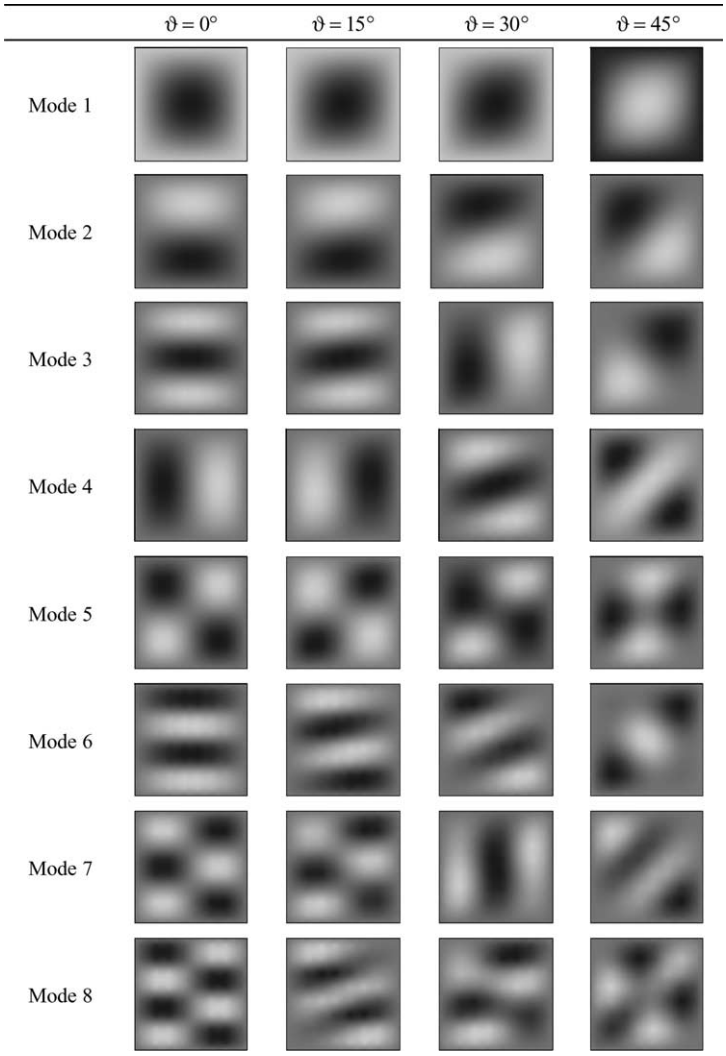

Fig. 5. Mode shapes for five-layer graphite/epoxy simply-supported square plates with $[\vartheta°/-\vartheta°/\vartheta°/-\vartheta°/\vartheta°]$ layup.

boundary and domain degrees of freedom. In particular, adding internal nodes unstiffs the plate, then one has convergence from above, whereas increasing the number of boundary nodes makes the plate more stiff and then one has convergence from below. Thus, a suitable choice of boundary and internal nodes affects the convergence rate, though computations evidence accurate results for different ratios of boundary and internal degrees of freedom. The accuracy of the approach has been firstly checked by comparing the computed frequency parameter for square plate with exact and numerical solutions (Vasiliev, 1993; Leissa and Narita, 1989; Chow et al., 1992; Han and Petyt, 1996). These results, shown in Tables 1 and 2, evidence excellent agreement with the literature solutions confirming the accuracy and the excellent convergence properties of the proposed method. This is able to determine the vibration frequencies with an error less than 0.5% for all the considered boundary conditions and anisotropy degree of the plate. Figs. 5 and 6 show the mode shapes of the analyzed plates. These mode shapes compare favorably with those presented in the literature (Chow et al., 1992; Hung et al., 1993) and they show the ability of the approach to correctly

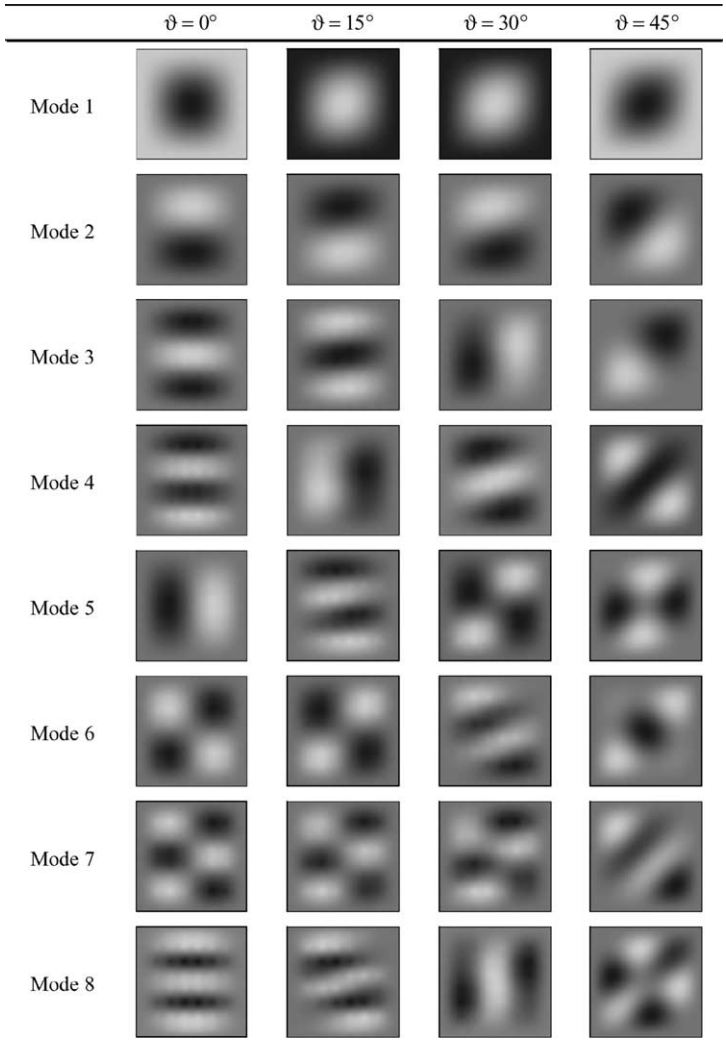

Fig. 6. Mode shapes for five-layer graphite/epoxy fully clamped square plates with $[\vartheta°/-\vartheta°/\vartheta°/-\vartheta°/\vartheta°]$ layup.

predict this fundamental part of the dynamic behavior. Again, different plate shapes have been considered to confirm the method capabilities. In particular some examples for trapezoidal, triangular and circular plates have been analyzed and the results compared with those of Liew (1992, 1994) and Liew and Chiam (1994). The computed vibration frequencies are shown in Tables 3–6 where the plate geometry and layup

Table 3
Natural frequency parameter λ of cantilever trapezoidal plates

	Mode[a]	c/a	Layup			
			A	B	C	D
$a/h=1$	1	2/5	3.56	3.57	3.32	2.99
			(3.55)	(3.59)	(3.33)	(2.96)
		4/5	2.96	3.00	2.82	2.49
			(2.96)	(3.02)	(2.96)	(2.49)
	2	2/5	8.68	11.27	11.28	12.01
			(8.67)	(11.25)	(11.24)	(12.02)
		4/5	5.18	7.04	6.99	7.54
			(5.18)	(7.06)	(6.98)	(7.57)
	3	2/5	18.58	18.85	17.47	15.39
			(18.41)	(18.72)	(17.32)	(15.38)
		4/5	17.87	17.73	16.66	14.36
			(17.60)	(17.81)	(16.49)	(14.65)
	4	2/5	27.02	31.28	32.13	32.31
			(26.58)	(31.39)	(31.45)	(32.44)
		4/5	21.39	22.84	22.69	23.85
			(20.94)	(22.89)	(23.63)	(24.15)
	5	2/5	38.65	39.02	39.25	39.46
			(38.27)	(42.79)	(45.22)	(40.91)
		4/5	22.45	25.47	24.61	25.07
			(22.33)	(25.48)	(23.63)	(26.71)
	6	2/5	49.94	50.24	44.70	46.66
			(49.17)	(49.41)	(45.74)	(47.89)
		4/5	34.28	39.99	45.94	42.07
			(33.96)	(41.66)	(46.15)	(41.80)

A) $[0°/90°/90°/0°]_s$
B) $[22.5°/-22.5°/67.5°/-67.5°]_s$
C) $[(0°/45°/-45°/90°)_2]_s$
D) $[(30°/-30°/60°/-60°)_2]_s$

[a] The values in parentheses are adapted from Liew (1992).

Table 4
Natural frequency parameter λ of symmetrically five-layer cantilever isosceles triangular plates

	Mode[a]	ϑ				
		0°	30°	45°	60°	90°
$[\vartheta°/-\vartheta°/\vartheta°/-\vartheta°/\vartheta°]$	1	1.808	2.416	3.795	4.915	6.418
		(1.813)	(2.423)	(3.538)	(4.925)	(6.386)
$a/h=1$	2°	7.826	10.125	14.625	18.087	16.681
		(7.870)	(10.283)	(14.490)	(18.058)	(16.479)
	3	10.321	17.200	20.536	23.036	27.318
		(10.320)	(17.263)	(20.540)	(23.078)	(27.094)
	4	18.995	24.975	35.921	42.601	39.307
		(19.157)	(25.403)	(35.896)	(42.499)	(38.624)
	5	26.064	39.891	47.900	53.879	46.562
		(26.043)	(40.393)	(47.699)	(53.674)	(45.747)
	6	35.061	47.590	62.772	59.245	67.896
		(35.401)	(48.337)	(62.215)	(59.283)	(65.880)

[a] The values in parentheses are adapted from Liew and Chiam (1994).

Table 5
Natural frequency parameter λ of symmetrically five-layer cantilever right triangular plates

	Mode[a]	ϑ				
		0°	30°	45°	60°	90°
$[\vartheta°/-\vartheta°/\vartheta°/-\vartheta°/\vartheta°]$ $a/h=1$ 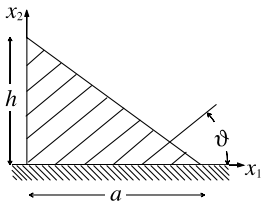	1	1.678	2.192	3.072	3.944	5.319
		(1.677)	(2.196)	(3.037)	(3.980)	(5.282)
	2°	7.072	9.197	12.312	14.489	13.703
		(7.071)	(9.245)	(12.303)	(14.458)	(13.563)
	3	10.874	15.751	19.485	22.890	26.810
		(10.867)	(15.868)	(19.278)	(22.719)	(26.724)
	4	17.506	22.261	28.826	30.743	30.391
		(17.495)	(22.410)	(28.644)	(30.614)	(30.020)
	5	26.315	33.616	40.462	46.671	45.268
		(26.267)	(34.204)	(40.197)	(46.401)	(44.625)
	6	33.385	42.789	53.605	55.308	56.114
		(33.305)	(43.233)	(53.388)	(55.031)	(55.938)

[a] The values in parentheses are adapted from Liew and Chiam (1994).

Table 6
Natural frequency parameter λ of symmetrically 16-layer clamped circular plates

	Mode[a]	ϑ			
		0°	15°	30°	45°
$[(\vartheta°/-\vartheta°)_4]_S$ 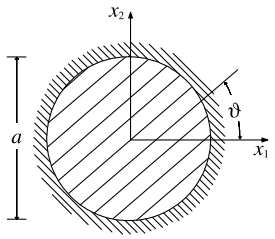	1	26.619	26.713	26.821	26.862
		(26.354)	(26.518)	(26.718)	(26.783)
	2°	36.922	39.902	46.935	52.966
		(36.680)	(39.696)	(46.788)	(52.832)
	3	52.097	57.978	63.385	58.569
		(51.858)	(57.755)	(63.076)	(58.416)
	4	68.665	67.511	72.695	86.034
		(67.775)	(66.885)	(72.476)	(85.750)
	5	72.323	81.167	93.078	92.831
		(72.013)	(80.843)	(92.691)	(92.552)
	6	82.957	86.987	104.82	107.93
		(82.086)	(86.273)	(104.44)	(107.56)

[a] The values in parentheses are adapted from Liew (1994).

characteristics are given for each case. Also these results show good agreement with those existing in the literature. The computations performed underline the computational efficiency of the proposed approach as compared to the other numerical methods. Indeed, focusing for example on the case of clamped rectangular plates, the accuracy of the presented results has been obtained with 100 degrees of freedom and 40 shadow boundary elements to compute the influence coefficients. By using conventional finite elements the same level of accuracy can be obtained by using at least a double number of degrees of freedom and elements (e.g. ANSYS results given in Han and Petyt, 1996). On the other hand, due to the reduction in the problem dimensionality, the classical boundary element method allows to model the plate behavior with a number of unknowns and elements similar to those of the present formulation. Nevertheless, it presents computational complexities associated with singular kernels, lack of symmetry and definiteness of the structural operators and resulting non-standard eigenvalue problems (Kitahara, 1985). The DBM, proposed in this paper, has the dimensionality characteristic of a boundary element model and an high computational efficiency related to a symmetric and definite standard resolving system whose influence coefficients are calculated by performing boundary integrals of regular kernels only. In conclusion the presented examples prove the

effectiveness of the proposed method whose features described in the previous sections make it very appealing from the numerical and computational point of view.

8. Conclusions

A new meshfree method for anisotropic plate dynamics has been presented. The method is based on a different view of the so-called DBM previously presented by the authors for isotropic plates in the framework of the boundary elements approaches. The model derived in this paper presents many advantages with respect to the more common field methods such as finite elements and finite differences and to the classical boundary element methods. These advantages can be summarized as follows: (i) No connectivity is needed because the discretization process is based on the employment of a set of randomly distributed boundary and internal nodes. (ii) The formulation preserves the symmetry and definiteness properties of the continuum in the discrete structural operators that is the stiffness and mass matrix are symmetric and positive definite. (iii) The mass matrix is frequency-independent and due to the operators properties the resolving system allows the employment of standard and computationally efficient numerical procedures. (iv) The approach has the dimensionality of a boundary element model and it involves nodal displacements only. (v) The method has meaningful computational advantages associated with the definition of the influence coefficients in terms of boundary integrals of regular kernels. (vi) The method is very suitable for computer implementation. The method has been tested by performing the analysis on classical laminated composite plates. These numerical examples have shown the accuracy and excellent convergence of the results, which prove the effectiveness of the approach. The above-mentioned features are surely attractive so that this method deserves consideration for the solution of problems involving anisotropic plate dynamics.

Acknowledgement

The authors would like to thank Eng. Ivano Benedetti for his assistance during the development of the computer code.

References

Atluri, S.N., Zhu, T., 2000. New concepts in meshless methods. International Journal for Numerical Methods in Engineering 47 (1–3), 537–556.

Belytschko, T., Lu, Y.Y., Gu, L., 1994. Element-free Galerkin methods. International Journal for Numerical Methods in Engineering 37 (2), 229–256.

Belytschko, T., Krongauz, Y., Organ, D., Fleming, M., Krysl, P., 1996. Meshless methods: an overview and recent developments. Computer Methods in Applied Mechanics and Engineering 139 (1–4), 3–47.

Chati, M.K., Mukherjee, S., Mukherjee, Y.X., 1999. The boundary node method for three-dimensional linear elasticity. International Journal for Numerical Methods in Engineering 46 (8), 1163–1184.

Chow, S.T., Liew, K.M., Lam, K.Y., 1992. Transverse vibration of symmetrically laminated rectangular composite plates. Composite Structures 20 (4), 213–226.

Davì, G., Milazzo, A., 1994. A symmetric and positive definite variational BEM for 2-D free vibration analysis. Engineering Analysis with Boundary Elements 14 (4), 343–348.

Davì, G., Milazzo, A., 1997a. A symmetric and positive definite BEM for 2-D forced vibrations. Journal of Sound and Vibrations 206 (4), 611–617.

Davì, G., Milazzo, A., 1997b. A new symmetric and positive definite boundary element formulation for lateral vibration of plates. Journal of Sound and Vibrations 206 (4), 507–521.

Davì, G., Milazzo, A., Marretta, R.M., 1997. Panel flutter by a symmetric and positive definite BEM formulation. In: Proceedings of the International Forum on Aeroelasticity and Structural Dynamics, vol. III, Rome, pp. 151–158.

Davì, G., Milazzo, A., 1999. Displacement boundary method for orthotropic plates. In: Proceedings of the XXI Boundary Element Method Conference. Computational Mechanics Publications, Southampton, pp. 671–680.

De Figueredo, T.G.B., Brebbia, C.A., 1989. A new hybrid displacement variational formulations of BEM for elastostatics. In: Proceedings of the 11th International Conference on BEM. Computational Mechanics Publications and Springer Verlag, Southampton and Berlin, pp. 47–57.

Han, W., Petyt, M., 1996. Linear vibration analysis of laminated rectangular plates using the hierarchical finite element method—I. Free vibration analysis. Computers and Structures 61 (4), 705–712.

Hearmon, R.F.S., 1959. The frequency of flexural vibration of rectangular orthotropic plates with clamped and supported edges. Journal of Applied Mechanics 26 (2), 537–540.

Hung, K.C., Liew, K.M., Lim, M.K., Leong, S.L., 1993. Boundary beam characteristics orthonormal polynomials in energy approach for vibration of symmetric laminates—I: Classical boundary conditions. Composite Structures 26 (3–4), 167–184.

Irschik, H., 1984. A boundary-integral equation method for bending of orthotropic plates. International Journal Solids Structures 20 (3), 245–255.

Kabir, H.R.H., Al-Khaleefi, A.M., Chaudhuri, R.A., 2001. Free vibration analysis of thin arbitrarily laminated anisotropic plates using boundary-continuous displacement Fourier approach. Composite Structures 53 (4), 469–476.

Kansa, E.J., 1990. Multiquadrics—a scattered data approximation scheme with applications to computational fluid dynamics: II. Solutions to parabolic, hyperbolic and elliptic partial differential equations. Computers and Mathematics with Applications 19 (8–9), 147–161.

Kitahara, M., 1985. Boundary Integral Equation Methods to Eigenvalue Problems of Elastodynamics and Thin plates. Elsevier.

Krysl, P., Belytschko, T., 1995. Analysis of thin plates by the element-free Galerkin method. Computational Mechanics 17 (1–2), 26–35.

LaMattina, B., Klang, E.C., Eischen, J.W., 1998. A study of solutions for the anisotropic plate subjected to a concentrated force. Journal of Applied Mechanics 65 (2), 273–276.

Leissa, A.W., Narita, Y., 1989. Vibration studies for simply supported symmetrically laminated rectangular plates. Composite Structures 12 (2), 113–132.

Leitao, V.M.A., 2001. A meshless method for Kirchhoff plate bending problems. International Journal for Numerical Methods in Engineering 52 (10), 1107–1130.

Lekhnitskii, S.G., 1968. Anisotropic Plates. Gordon and Breach, New York.

Liew, K.M., 1992. Vibration of symmetrically laminated cantilever trapezoidal composite plates. International Journal of Mechanical Science 34 (4), 299–308.

Liew, K.M., 1994. Vibration of clamped circular symmetric laminates. ASME Journal of Vibration and Acoustics 116 (2), 141–145.

Liew, K.M., Chiam, T.C., 1994. The free flexural vibration of symmetric angle-ply triangular composite laminates. Journal of Sound and Vibrations 169 (5), 633–654.

Liew, K.M., Xiang, Y., Kitipomchai, S., 1995. Research on thick plate vibrations: a literature survey. Journal of Sound and Vibration 180 (1), 163–176.

Liew, K.M., Lim, H.K., Tan, M.J., He, X.Q., 2002a. Analysis of laminated composite beams and plates with piezoelectric patches using the element-free Galerkin method. Computational Mechanics 29 (6), 486–497.

Liew, K.M., Ng, T.Y., Zhao, X., Reddy, J.N., 2002b. Harmonic reproducing kernel particle method for free vibration analysis of rotating cylindrical shells. Computer Methods in Applied Mechanics and Engineering 191 (37–38), 4141–4157.

Liew, K.M., Wu, H.Y., Zou, G.P., Ng, T.Y., 2002c. Elasto-plasticity revisited: numerical analysis via reproducing kernel particle method and parametric quadratic programming. International Journal for Numerical Methods in Engineering 55 (6), 669–683.

Liew, K.M., Ng, T.Y., Wu, H.Y., 2002d. Meshfree method for large deformation analysis—a reproducing kernel particle approach. Engineering Structures 24 (5), 453–551.

Liew, K.M., Wu, H.Y., Ng, T.Y., 2002e. Meshless method for modeling of human proximal femur: treatment of nonconvex boundaries and stress analysis. Computational Mechanics 28 (5), 390–400.

Liszka, T., 1984. An interpolation method for irregular net of nodes. International Journal for Numerical Methods in Engineering 20 (9), 1599–1612.

Liu, W.K., Jun, S., Li, S., Adee, J., Belytschko, T., 1995. Reproducing kernel particle methods for structural dynamics. International Journal for Numerical Methods in Engineering 38 (10), 1655–1679.

Monaghan, J.J., 1982. An introduction to SHP. Computer Physics Communications 48 (1), 89–96.

Mossakowski, J., 1995. Singular solutions of anisotropic plates. Archiwum Mechaniki. Stosowanej 7 (1), 97–110, in Polish.

Nayroles, B., Touzot, G., Villon, P., 1992. Generalizing the finite element method: diffuse approximation and diffuse elements. Computational Mechanics 10 (5), 307–318.

Noor, A.K., Burton, W.S., 1989. Assessment of shear deformation theories for multilayered composite plates. Applied Mechanics Reviews 42 (1), 1–13.

Providakis, C.P., Beskos, D.E., 1999. Dynamic analysis of plates by boundary elements. Applied Mechanics Reviews 52 (7), 213–236.

Reddy, J.N., Robbins Jr., D.H., 1994. Theories and computational models for laminated composite laminates. Applied Mechanics Reviews 47 (6), 147–169.

Rossi, R.E., Bambill, D.V., Laura, A.A., 1998. Vibrations of a rectangular orthotropic plate with a free edge: comparison of analytical and numerical results. Ocean Engineering 25 (7), 521–527.

Shi, G., Bezine, G., 1988. A general boundary integral formulation for the anisotropic plate bending problems. Journal of Composite Materials 22 (6), 694–716.

Shuyao, L., 2002. A research on the companion solution for a thin plate in the meshless local boundary integral equation method. Engineering Analysis with Boundary Elements 26 (6), 505–509.

Suchar, M., 1964. On singular solutions in the theory of anisotropic plates. Bulletin de l'Academie Polonaise des Sciences. Serie des Sciences Techniques 12, 29–38.

Vasiliev, V.V., 1993. Mechanics of Composite Structures. Taylor & Francis, Washington.

Wu, B.C., Altiero, N.J., 1981. A new numerical method for the analysis of anisotropic thin-plate bending problems. Computer Methods in Applied Mechanics and Engineering 25 (3), 343–353.

Zhang, J., Yao, Z., Li, H., 2002. A hybrid boundary node method. International Journal for Numerical Methods in Engineering 53 (1), 751–763.

Zhu, T., Zhang, J., Atluri, S.N., 1999. A meshless numerical method based on the local boundary integral equation (LBIE) to solve linear and non-linear boundary value problems. Engineering Analysis with Boundary Elements 23 (5–6), 375–389.